Iraqi Journal of Physics, 2019 *Vol.17, No.43, PP. 1-10*
DOI: 10.20723/ijp.17.43.1-10

Study of charge density distributions and elastic electron scattering cross sections for some stable nuclei

Rafah Ismail Noori[1] and Arkan R. Ridha[2]

[1]Department of Physics, Education College of Pure Science -Ibn Al-Haithem, Baghdad University

[2]Department of Physics, College Science, University of Baghdad

E-mail: 07710638947rf@gmail.com

Abstract

In this work, the charge density distributions and elastic electron scattering cross sections have been calculated for stable ^{10}B, ^{19}F, ^{20}Ne, ^{27}Al and ^{31}P nuclei. The radial wave functions of Woods-Saxon potential are used to fulfill the calculations in shell model. The parameters of Woods-Saxon potential are fixed so as to regenerate the available experimental size radii and single-nucleon binding energy of the last proton and neutron on Fermi's surface, besides, The configuration mixing have been applied using CKII (for ^{10}B) and SDBA (for ^{19}F, ^{20}Ne, ^{27}Al and ^{31}P) interactions.

Key words
Charge density distributions, size radii, elastic electron scattering cross section.

Article info.
Received: Jun. 2019
Accepted: Aug. 2019
Published: Dec. 2019

دراسة توزيعات الكثافة الشحنية ومساحة المقطع العرضي للاستطارة الالكترونية المرنة من بعض النوى المستقرة

رفاه اسماعيل نوري[1] و اركان رفعة رضا[2]

[1]قسم الفيزياء، كلية التربية للعلوم الصرفة ابن الهيثم، جامعة بغداد

[2]قسم الفيزياء، كلية العلوم، جامعة بغداد

الخلاصة

في هذا العمل، تم حساب توزيعات كثافة الشحنة ومساحة المقطع العرضي للاستطارة الالكترونية المرنة من بعض النوى المستقرة (^{10}B, ^{19}F, ^{20}Ne, ^{27}Al و^{31}P). استخدمت الدوال الموجية لجهد وود- ساكسون لعمل الحسابات بانموذج القشرة. ثبتت معلمات جهد وود- ساكسون بحيث تولد انصاف الاقطار النووية المتوفرة عمليا" وكذلك طاقة الربط للبروتون والنيوترون الاخير الموجود على سطح فيرمي. بالاضافة الى ما ذكر اعلاه، تم استخدام التشكيلات المختلطة ما بين القشرالفرعية بأستخدام تفاعل كوهيين- كوراث (^{10}B) وتفاعل اس-دي-بي-اي (^{19}F و ^{20}Ne و ^{27}Al و ^{31}P).

Introduction

The nuclear charge radius is one of the most clear and important nuclear quantities that give information about the nuclear shell model since they are directly related to the wave functions of protons, and the effect of effective interactions on nuclear structure. The charge density distribution (CDD) is one of the many important quantities in the nuclear structure which have been well studied experimentally over a vast range of nuclei [1,2] and can be measured accurately from high energy electron elastic scattering. Beside electron scattering, some of the charge sensitive methods such as Coulomb effects in mirror nuclei, p-mesonic atoms and p-meson scattering, Isotope shifts are applicable [3]. The causes of using electron scattering are due to the fact that the electron is a point-like particle, and probes nuclei through the well electromagnetic interaction. In stable nuclei, the density distributions of protons and neutrons are homogeneously mixed in the nucleus, namely $\rho_P(r) \propto \rho_n(r)$ and surface thickness is constant [4]. The proton and the neutron potentials are the same except for the Coulomb potential. Only the existence of the Coulomb potential makes the radius of protons slightly smaller. Therefore, no thick neutron skin is expected for stable nuclei even if they have large (N- Z) values [5]. For ^{10}B in Ref. [6], the longitudinal and transverse form factors were calculated of the low-lying levels using Woods-Saxon (WS) potential which was found to provide a much better representation of the data than the harmonic-oscillators (HO) model. For ^{20}Ne in Ref. [7], the charge and matter distributions were calculated taking into account complex configuration mixing using semi-self-consistent approach with WS potential. In Ref. [8] the large-basis shell-model wavefunctions of WS and HO were used to analyze the longitudinal and transverse form factors. For ^{31}P, in Ref. [9] the electorn scattering cross-sections, charge form factors and charge distributions were studied using Hartree-Fock (HF) calculations performed in a spherical basis and in an axially deformed basis. The single-particle wave functions of Woods-Saxon (WS) potential were used with very good agreements with experimental data for both stable [10, 11] and exotic nuclei [12]. For results in Refs. [10, 11], the WS parameters are applied to ^{4}He, ^{12}C and ^{16}O, besides ^{40}Ca and ^{48}Ca with different parameters for each subshell of the nuclei in their both study. In Ref. [12], the approach of HO+WS has been applied to exotic ^{11}Be, ^{19}C and ^{11}Li with very good agreements with experimental data. The transformed HO wave functions in local-scale transformation were opened a new approach and used to repair the performance of the radial wave functions for both stable and halo nuclei [13-15].

Therefore, in the present work, we undertook the computation of charge density distributions, rms radii and elastic electron scattering cross sections for stable ^{10}B, ^{19}F, ^{20}Ne, ^{27}Al and ^{31}P nuclei using the radial wave functions of WS potential in shell model approach. The configurations mixing have been adopted and the Fermi's surfaces for nuclei under study are shifted up words to the last subshell of the active model space used for each studied nuclei. This work is programmed using Fortran power station 90 to solve the radial Schrodinger's equation.

Theoretical formulations

The operator of density distribution for *A*-nucleon system can be written as [16]

$$\hat{\rho}_{t_z}(\vec{r}) = \sum_{i=1}^{A} e_{t_z}(i) e_{t_z} \delta(\vec{r} - \vec{r}_i) \qquad (1)$$

where $\delta(\vec{r} - \vec{r}_i)$ is Dirac delta function, and t_z represent the single-nucleon isospin quantum number ($t_z = 1/2$ for protons) ($t_z = -1/2$ for neutrons). Eq. (1) can be simplified after writing Dirac delta function in spherical coordinates as [17]:

$$\hat{\rho}_{t_z}(\vec{r}) = \sum_{k=1}^{A} e_{t_z}(k) \frac{\delta(r-r_k)}{r_k^2} \sum_{JM} Y_{JM}(\Omega_{r_k}) Y_{JM}^*(\Omega_r) \quad (2)$$

The matrix element to Eq.(2) the yield will be:

$$\rho_{t_z}(\boldsymbol{r}) = \langle J_f M_f | \hat{\rho}_{t_z}(\vec{r}) | J_i M_i \rangle = \sum_{JM} (-1)^{J_f - M_f} \begin{pmatrix} J_f & J & J_i \\ -M_f & M & M_i \end{pmatrix} Y_{JM}^*(\Omega_r)\, \rho_{J,t_z}(r) \quad (3)$$

where $\rho_{J,t_z}(r)$ represents transition density distribution and can be simplified to:

$$\rho_{J,t_z}(r) = \frac{1}{\sqrt{4\pi}} \frac{1}{\sqrt{2J_i+1}} \sum_{ab} X_{b,a,t_z}^{J_f,J_i,J} \langle j_b \| Y_J \| j_a \rangle R_{n_b l_b}(r, b_{t_z}) R_{n_a l_a}(r, b_{t_z}) \quad (4)$$

The total charge density distribution $\rho_{ch}(r)$ is coming from the folding of protons and neutrons [18]

$$\rho_{ch}(r) = \rho_{ch,t_z=1/2}(r) + \rho_{ch,t_z=-1/2}(r) \quad (5)$$

where

$$\rho_{ch,t_z=1/2}(r) = \int \rho_{J=1/2}(r) \rho_{Pr}(r - \acute{r}) d\grave{r} \quad (6)$$

and

$$\rho_{ch,t_z=-1/2}(r) = \int \rho_{J=-1/2}(r) \rho_{neu}(r - \acute{r}) d\grave{r} \quad (7)$$

$$\rho_{pr}(r) = \frac{1}{(\sqrt{\pi} a_{pr})^3} e^{\left(\frac{-r^2}{a_{pr}^2}\right)} \quad (8)$$

and

$$\rho_{neu}(r) = \frac{1}{(\pi r_i^2)^{3/2}} \sum_1^2 \theta_i\, e^{-r^2/r_i^2} \quad (9)$$

In Eqs. (5) and (7), $a_{pr} = 0.65\, fm$ [19], the parameters θ_i and r_i are tabulated in ref. [18].

To calculate the nuclear charge form factor, one has to take the Fourier transform to CDD as follows:

$$F_{ch}(q) = \frac{1}{Z} \int \rho_{J,ch}(r) e^{i\vec{q}.\vec{r}}\, d\vec{r} \quad (10)$$

q is the momentum transfer to the nucleus.The differential cross- section of the scattering of electron from a nucleus of charge (Ze) and mass (M) through infinitesimal solid angle $(d\Omega)$ in plane-wave Born approximation (PWBA) is given by [2, 19]

$$\frac{d\sigma}{d\Omega} = \left(\frac{d\sigma}{d\Omega}\right)_{Mott} |F(q)|^2 \quad (11)$$

where $\left(\frac{d\sigma}{d\Omega}\right)_{Mott}$ represents the Mott cross section for the scattering of high-energy electron from point nucleus and it is related to the Rutherford cross section by the following relationship:

$$\left(\frac{d\sigma}{d\Omega}\right)_{Mott} = \left(\frac{d\sigma}{d\Omega}\right)_{Rutheford} \left[1 - \beta^2 \sin^2\left(\frac{\theta}{2}\right)\right] \quad (12)$$

where

$$\left(\frac{d\sigma}{d\Omega}\right)_{Rutheford} = \left(\frac{Z\alpha}{2E_0}\right)^2 \frac{(\hbar c)^2}{\sin^4\left(\frac{\theta}{2}\right)} \quad (13)$$

β is very close to unity because of the high energy of electron, so that, the factor $1 - \beta^2 \sin^2\left(\frac{\theta}{2}\right) \approx cos^2(\frac{\theta}{2})$, therefore, Eq.(12) reduces to

$$\left(\frac{d\sigma}{d\Omega}\right)_{Mott} = \frac{Z^2 \alpha^2 \cos^2 \frac{\theta}{2}}{4E_0^2 \sin^4 \frac{\theta}{2}} \quad (14)$$

α is the fine-structure constant, θ is the electron scattering angle, E_o represents the energy of the incident electrons. The Mott cross section has Z^2 dependence, it becomes infinity at a scattering angle zero, which is a common feature of Coulomb scattering and it becomes zero at scattering angle of 180°. The Mott cross section is found to have direct relationship with E_0^2 inverse relationship with q^4.

Results and discussion

The radial wave functions of WS potential have been used in shell model approach to calculate the charge density distributions, rms radii and elastic electron scattering cross sections for ^{10}B, ^{19}F, ^{20}Ne, ^{27}Al and ^{31}P nuclei. The parameters of WS potential (U_0, r_0, a_0, $r_{s.o.}$ and $a_{s.o.}$) are displayed in Table 1. They are chosen so as to reproduce the experimental single-nucleon binding energies (for the last proton and neutron on Fermi surface) and available experimental rms radii for nuclei under study. The depth of spin-orbit ($U_{s.o.}$) is fixed to 9.0 MeV.

The properties of nuclei in aspect of spin, parity, and isospin are tabulated in Table 2.

In Table 3, the calculated and available experimental rms radii for stable nuclei under study are displayed. It is clear that the experimental data are well generated for the fixed WS parameters mentioned in Table 1. In Tables 4-8, the single binding energies of protons and neutrons predicted by the fixed parameters of WS potential are presented for ^{10}B, ^{19}F, ^{20}Ne, ^{27}Al and ^{31}P nuclei. It is obvious that the last single nucleon binding energies for both protons and neutrons are well reproduced.

Table 1: Parameters of Woods-Saxon potential for stable $^{10}_{5}B_{5}$, $^{19}_{9}F_{10}$, $^{20}_{10}Ne_{10}$, $^{27}_{13}AL_{14}$ and $^{31}_{15}P_{16}$ nuclei.

$^{A}_{Z}X_{N}$		U_0 (MeV)	r_0 (fm)	a_0 (fm)	$U_{s.o.}$ (MeV)	$r_{s.o.}$ (fm)	$a_{s.o.}$ (fm)
$^{10}_{5}B_{5}$	Neutrons	58.461	1.300	0.550	9.0	1.300	0.550
	Protons	50.552	1.400	0.350	9.0	1.400	0.350
$^{19}_{9}F_{10}$	Neutrons	78.831	1.200	0.750	9.0	1.200	0.750
	Protons	68.118	1.35	1.050	9.0	1.35	1.050
$^{20}_{10}Ne_{10}$	Neutrons	69.213	1.430	0. 850	9.0	1.430	0. 850
	Protons	66.794	1.50	1.00	9.0	1.50	1.00
$^{27}_{13}AL_{14}$	Neutrons	64.636	1.20	0.450	9.0	1.20	0.450
	Protons	63.817	1.270	0.75	9.0	1.270	0.75
$^{31}_{15}P_{16}$	Neutrons	55.924	1.280	0.650	9.0	1.280	0.650
	Protons	54.443	1.30	0.550	9.0	1.30	0.550

Table 2: J^{π}, T for stable nuclei under study [28].

$^{A}_{Z}X_{N}$	$J^{\pi}T$
$^{10}_{5}B_{5}$	$3^{+}0$
$^{19}_{9}F_{10}$	$1/2^{+}\frac{1}{2}$
$^{20}_{10}Ne_{10}$	$0^{+}0$
$^{27}_{13}AL_{14}$	$5/2^{+}\frac{1}{2}$
$^{31}_{15}P_{16}$	$1/2^{+}\frac{1}{2}$

Table 3: Calculated rms radii for stable nuclei compared with available eperimentl data.

${}^{A}_{Z}X_N$	$\langle r_p^2\rangle^{1/2}$ fm	Exp. $\langle r_p^2\rangle^{1/2}$ fm	$\langle r_n^2\rangle^{1/2}$ fm	Exp. $\langle r_n^2\rangle^{1/2}$ fm	$\langle r_{ch}^2\rangle^{1/2}$ fm	Exp. $\langle r_{ch}^2\rangle^{1/2}$ fm	$\langle r_m^2\rangle^{1/2}$ fm	Exp. $\langle r_m^2\rangle^{1/2}$ fm
${}^{10}_{5}B_5$	2.388	-	2.335	-	2.498	2.45 ± 0.12 [29]	2.362	2.56 ± 0.23 [30]
${}^{19}_{9}F_{10}$	2.812	-	2.5	-	2.903	2.90 ± 0.02 [29]	2.652	2.61 ± 0.07 [31]
${}^{20}_{10}Ne_{10}$	2.944	-	2.767	-	3.033	3.0413 ± 0.025 [29]	2.857	2.87 ± 0.03 [31]
${}^{27}_{13}AL_{14}$	2.949	-	2.719	-	3.036	3.035±0.002 [29]	2.832	-
${}^{31}_{15}P_{16}$	3.112	-	3.078	-	3.195	3.19±0.03 [29]	3.095	-

Table 4: Single-nucleon binding energies for ^{10}B.

State	Single-neutron binding energy (MeV)	Single-proton binding energy (MeV)
$1s_{1/2}$	-31.819	-27.976
$1p_{3/2}$	-15.370	-13.289
$1p_{1/2}$	-8.437 [28]	-6.587 [28]

Table 5: Single-nucleon binding energies for ^{19}F.

State	Single-neutron binding energy (MeV)	Single-proton binding energy (MeV)
$1s_{1/2}$	-51.651	-38.796
$1p_{3/2}$	-35.187	-26.003
$1p_{1/2}$	-30.025	-22.249
$1d_{5/2}$	-18.804	-13.612
$2s_{1/2}$	-15.690	-12.219
$1d_{3/2}$	-10.432 [28]	-7.994 [28]

Table 6: Single-nucleon binding energies for ^{20}Ne.

State	Single-neutron binding energy (MeV)	Single-proton binding energy (MeV)
$1s_{1/2}$	-49.052	-41.543
$1p_{3/2}$	-36.173	-29.873
$1p_{1/2}$	-32.656	-26.683
$1d_{5/2}$	-23.044	-18.162
$2s_{1/2}$	-20.000	-15.976
$1d_{3/2}$	-16.865[28]	-12.843 [28]

Table 7: Single-nucleon binding energies for ^{27}Al.

State	Single-neutron binding energy (MeV)	Single-proton binding energy (MeV)
$1s_{1/2}$	-48.47	-39.266
$1p_{3/2}$	-35.393	- 27.258
$1p_{1/2}$	-31.523	-23.573
$1d_{5/2}$	-21.309	-14.884
$2s_{1/2}$	-14.824	-11.378
$1d_{3/2}$	-13.058[28]	- 8.271[28]

Table 8: Single-nucleon binding energies for ^{31}P.

State	Single-neutron binding energy (MeV)	Single-proton binding energy (MeV)
$1s_{1/2}$	-41.161	-34.616
$1p_{3/2}$	-30.192	-24.54
$1p_{1/2}$	-26.978	-21.488
$1d_{5/2}$	-18.629	-13.64
$2s_{1/2}$	-14.445	-8.679
$1d_{3/2}$	-12.311[28]	-7.297[28]

In Fig. 1, the calculated CDDs for ^{10}B, ^{19}F, ^{20}Ne, ^{27}Al and ^{31}P nuclei are displayed in Figs. 1 (a, b, c, d, e), respectively. The one-body density matrix elements needed to fulfil calculations in shell model are obtained using the nuclear shell model oxbash [20].

For ^{10}B, the CKII interaction [21] is used while for ^{19}F, ^{20}Ne, ^{27}Al and ^{31}P nuclei, the SDBA interaction [22] is adopted. The calculated results for ^{19}F, ^{20}Ne and ^{31}P nuclei are in very good agreement with experimental data. The calculated results for ^{10}B is underestimated the experimental data at central region on contrary to the results of ^{27}Al which overestimated the experimental data.

The calculated electron scattering cross sections for ^{10}B, ^{19}F, ^{20}Ne, ^{27}Al and ^{31}P nuclei are depicted in Fig. 2. Unfortunately, there are no available experimental data for ^{10}B, ^{19}F and ^{20}Ne nuclei to compare with. The experimental charge form factors for ^{10}B were calculated at incident energies, 198.5, 333 and 400 MeV [23]. For ^{19}F, the data were collected at energies from 78 and 340 MeV [24]. For ^{20}Ne the data were collected at 39.49, 65.93, 14.93 and 19.93 MeV [25]. The calculated electron scattering cross sections for ^{10}B, ^{19}F and ^{20}Ne depicted in Figs.2 (a, b, c), respectively showed direct relationship with energy. For ^{27}Al and ^{31}P, the experimental electron scattering cross section was collected at 250 and 500 MeV [26] and 250 and 400 MeV [27], respectively. The calculated cross sections are plotted in Fig.2 (d and e) for ^{27}Al and ^{31}P, respectively. Good agreements were obtained for both nuclei.

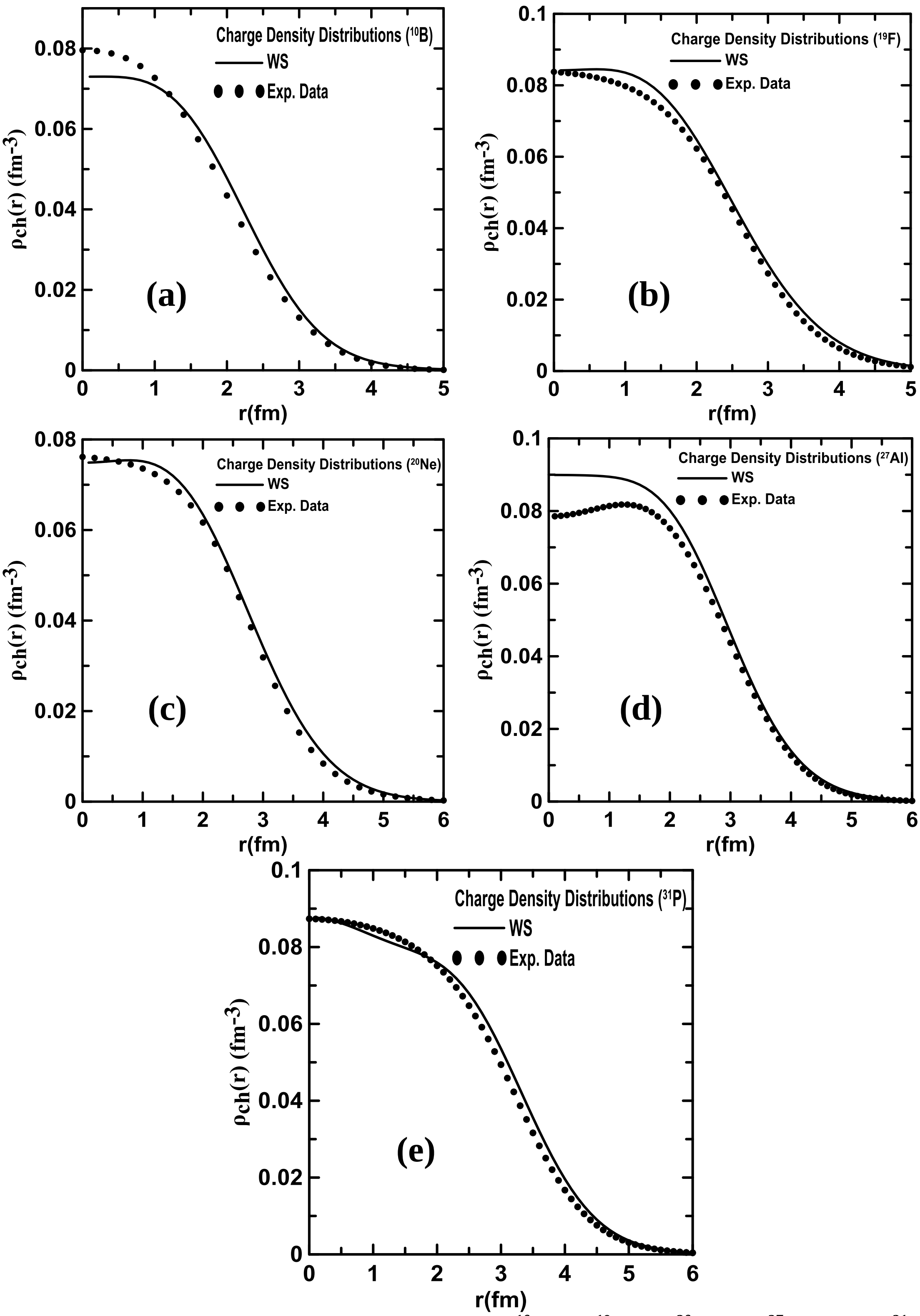

Fig. 1: Calculated charge density distributions for ^{10}B (a), ^{19}F (b), ^{20}Ne (c), ^{27}Al (d) and ^{31}P (e) the dotted symbols represent experimental data [29].

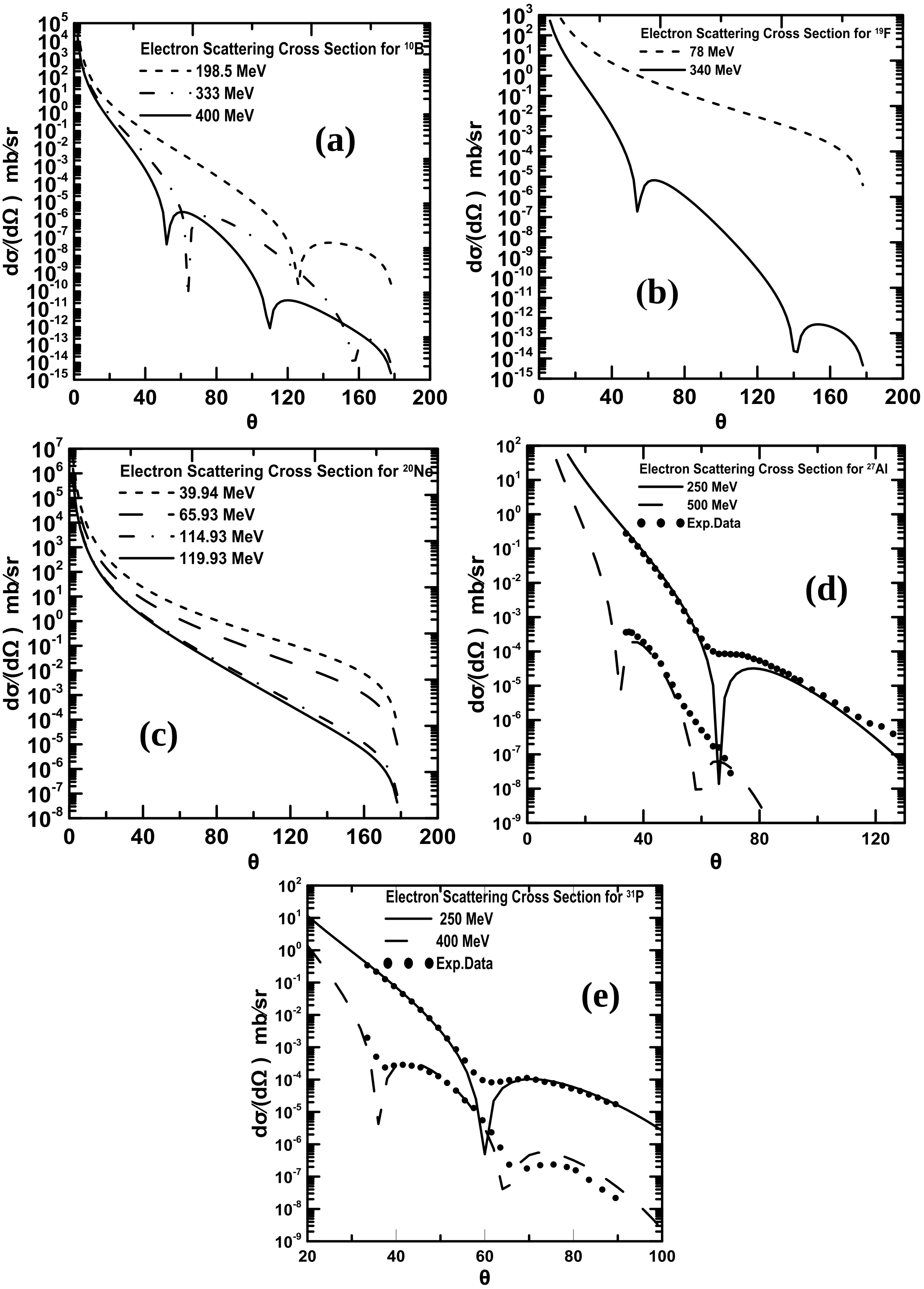

Fig. 2: Calculated electron scattering cross sections for ^{10}B (a) [23], ^{19}F (b) [24], ^{20}Ne (c) [25], ^{27}Al (d) [26] and ^{31}P (e) [27], respectively. The experimental data are presented by circles for ^{27}Al (d) and ^{31}P (e).

Conclusions

The theory of configuration mixing shell model is used to calculate charge density distributions (CDDs) and electron scattering cross section for stable ^{10}B, ^{19}F, ^{20}Ne, ^{27}Al and ^{31}P nuclei. The WS potential is adopted as a mean field potential to describe the movement of nucleons inside nucleus. The parameters of WS potential needed to obtain the realistic wavefunctions are fixed so as to reproduce the size radii and the last single proton and neutron binding energies on Fermi's surface. The Fermi's surfaces for chosen nuclei have been shifted upwordes to the last subshell of the active model space of the opted effective interactions to ensure the contribution from higher subshells. The calculated CDDs for stable nuclei under study are wholy in good agreement with experimental data. The calculated electron scattering cross section in plane wave Born approximation are also in good agreement with experimental data showing high energy dependence for incident electrons.

References

[1] C. J. Batty, E. Friedman, H. J. Gils, H. Rebel, Advances in Nuclear Physics, 19 (1989) 1-188.

[2] H. Uberall, Electron Scattering from Complex Nuclei, Part A Academic Press, New York, (1971) Chapter 5.

[3] Robert Hovstater, Electron Scattering and Nuclear Structure. Reviews of Modern Physics, 28 (1956) 214-254.

[4] Isao Tanihata, Nuclear Instruments and Methods in Physics Research, A 532 (2004) 79-85.

[5] K. Heyde, Basic Ideas and Concepts in Nuclear Physics, IOP Publishing Ltd, 2nd Ed. (1994).

[6] A. Cichocki, J. Dubach, R. S. Hicks, G. A. Peterson, C. W. De Jager, H. De Vries, N. Kalantar-Nayestanaki, T. Sato, Physical Review C, 51, (1995) 2406-2426.

[7] B. A. Brown, S. E. Massen and P. E. Hodgson, J.Phys. G: Nucl. Phys., 5 (1979) 1655-1698.

[8] R. P. Singhal, A. Watt, R. R., Whitehead, J.Phys. G: Nucl. Phys., 8 (1982) 1059-1083.

[9] J. Wesseling, C. W. de Jager, L. Lapikás, H. de Vries, L. W. Fagg, M. N. Harakeh, N. Kalantar-Nayestanaki, R. A. Lindgren, E. Moya De Guerra, P. Sarriguren, Physical Review C, 55, (1997). 2773-2786.

[10] A. R. Ridha, Iraqi Journal of Physics, 14 (2016) 42-50.

[11] A. R. Ridha, Journal of Al-Nahrain University, 20, 3 (2017) 83-90.

[12] A. R. Ridha and Z. M. Abbas, Iraqi Journal of Physics, 16 (2018) 29-38.

[13] A. R. Ridha and M. K. Suhayeb, Iraqi Journal of Science, 58, 4B (2017) 2098-2106.

[14] Saja H. Mohammed, A. R. Ridha, Iraqi Journal of Science, 59 (2018) 1866-1877.

[15] Saja H. Mohammed, Iraqi Journal of Physics, 16 (2018) 103-116.

[16] A. N. Antonov, P. E. Hodgson, I. Zh.Petkov, Nucleon Momentum and Density Distributions in Nuclei, Clarendon Press, Oxford (1988).

[17] G. R. Satchler, Direct Nuclear Reactions, Oxford University Press (1983).

[18] H. Chandra and G. Sauer, Phys. Rev., C 13 (1975) 245-252.

[19] L. R. B. Elton, Nuclear Sizes, Oxford University Press (1961).

[20] B.A. Brown, A. Etchegoyen, Rae W.D.M., Computer code OXBASH, MSU Cyclotron Laboratory Report No.524. (1986).

[21] S. Cohen, D. Kurath, Nucl. Phys., A 101, 1 (1967) 1-16.

[22] B. Alex Brown and W. A. Richter, Phys. Rev. C 74, 3 (2006) 034315.

[23] T. Stovall, J. Goldemberg, D. B. 1sbelle, Nuclear Physics, 86 (1966) 225-240.

[24] B.A. Brown and B.H. Wildenthal, Phys. Rev. C, Nuclear Physics, 32 (1985) 1127-1156.

[25] E. A. Knight, R. P. Singhal, R. G. Arthur, M .W. S. Macauley, J. Phys. G: Nucl. Phys., 7 (1981) 1115-1121.

[26] G. C. Li, M. R. Yearian and I. Sick, Phys. Rev., C9 (1974) 1861-1877.
[27] B. B. P. Sinha, G. A. Peterson, G. C Li., R. R. Whitney, Phys. Rev., C6 (1972) 1657- 1663.
[28] G. Audi, F. G. Kondev, Meng Wang, W.J. Huang, S. Naimi, Chinese Physics, C 41 (2017) 1-138.
[29] H. De Vries, C. W. De Jager, C. De Vries, (Nuclear Charge Density Distribution Parameters from Elastic Electron Scattering). Atomic Data and Nuclear Data Tables, 36 (1987) 495-536.
[30] A. Ozawa, T. Suzuki, I. Tanihata, Nuclear Physics, A 693 (2001) 32-62.
[31] A. Ozawa, O. Bochkarev, L. Chulkov, D. Cortina, H. Geissel, M. Hellström, M. Ivanov, R. Janik, K. Kimura, T. Kobayashi, A. A. Korsheninnikov, G. Münzenberg, F. Nickel, Y. Ogawa, A. A. Ogloblin, M. Pfützner, V. Pribora, Nuclear Physics, A 691, 3-4 (2001) 599-617.